Using AVO and LMR Analysis with DHI and Flat-Spot Calibration to Mitigate Reservoir Risk at Stonehouse, Offshore Nova Scotia

Bill Goodway*
EnCana, Calgary, AB
william.goodway@encana.com

and

Chris Szelewski, Steve Overell, Norm Corbett and Terry Skrypnek
EnCana, Calgary, AB, Canada

Summary

Amplitude variation with offset (AVO) and Lambda-Mu-Rho (LMR) attribute inversion have been successful in reducing reservoir risk in exploration drilling. However, AVO only detects relative anomalies due to high porosity hydrocarbon reservoirs while log-calibrated LMR inversion can provide a quantitative extraction of rock properties to discriminate lithology, porosity and fluids given reasonable data quality and amplitude preserved processing.

The motivation for AVO/LMR analysis on the Stonehouse 3D stems from the failure of the majority of Scotian slope wells drilled to intersect high porosity reservoir sands. In order to discriminate highly porous reservoir sands, various AVO/LMR responses to fluid and porosity variations were predicted through Gassmann Fluid Replacement Modelling (FRM) and porosity substitution of thin, low porosity target gas sands from the nearby Tantallon (M-41) well. Logs from the Annapolis (G-24) well provided background shear velocities and verification that higher porosity substitution of the M-41 sands matched the stratigraphically equivalent known gas sand in G-24. AVO synthetic gather wedge models ranging from zero to 50m thickness were created for the in-situ 9% porosity (Φ) and substituted 18%Φ cases, using various gas/brine saturations. The FRM predicted that high porosity substituted gas sands produce very bright AVO class 3 or 4 responses at thicknesses > 10m. By contrast, low porosity gas or brine sands had near zero contrast to background shales with dim AVO class 2 gather and stack responses, while the 18% Φ brine sands showed only marginal AVO class 1 contrast.

Beyond standard LMR ($\lambda\mu\rho$) cross-plotting that isolated gas sand clusters, an improved separation of high porosity sands was achieved using a $\lambda\rho - \mu\rho$ difference vs. acoustic P-impedance (Ip) template. Additionally a new, AVO class 6 fluid contact DHI is defined and the theoretical gradient model validated a structural flat-spot identified on the migrated stack by mapping its structural conformance to a salt dome flank. This DHI fluid contact control point was critical in the cross-plot data template masking and polygon projection onto the 3D volume. Along with further attribute analysis, the DHI template confirmed that trough-peak reflectors up-

dip from the flat-spot occupied the same cross-plot region as the 18% Φ gas sand model and were generally sparsely (hence discriminately) populated throughout the 3D.

Sand body depth volumes from LMR and AVO intercept-gradient reconnaissance were combined with independent, seismic-stratigraphic interpretation in GeoProbe enabling better-constrained resource estimates. The detailed AVO analysis also permitted a more confident assessment of the reservoir risk at the objective horizons.

Reprocessing, Interpretation and Mapping

The Stonehouse 3D covers a large, stratigraphic-structural prospect located on the Scotian slope, offshore Nova Scotia. The 3D was reprocessed to incorporate improved 3D demultiple methods (SRME) and pre-stack depth migration (PSDM). This new volume provided significantly improved imaging with broader bandwidth amplitude preservation that was now amenable to critical AVO/LMR analysis (Mojesky et al 2007).

Interpretation of the new data clearly identified submarine canyons/channels throughout the target Cretaceous section that could have transported coarse sediment to the Stonehouse prospect and these zones of interest were the focus of detailed AVO analysis. Figure 1 shows an arbitrary line from the volume with interpreted channels and 'geobodies' in the primary objective interval.

Figure 2 shows a postulated DHI flat-spot seen in the 12º-22º angle stack that was only evident after reprocessing and PSDM. AVO/LMR modelling and attribute inversion confirmed the flat-spot as being theoretically consistent with a new AVO class 6 classification of a true fluid contact. To the authors' knowledge, this level of understanding of AVO analysis for a fluid contact has not previously been published.

AVO and LMR Analysis: Modelling/Fluid Substitution

Petrophysical analysis of the M-41 well identified two, thin, low porosity sands in the Cretaceous Upper Missisauga Fm. interval that were gas-charged. A 10m, 9% Φ, 60% gas saturated sand at 5,200m MD was chosen for the fluid and porosity substitution. Figure 3 shows a LambdaRho ($\lambda\rho$) vs. MuRho ($\mu\rho$) cross-plot from the FRM along with the known G-24 gas sand and shale. Dipole logs over equivalent stratigraphic and depth ranges in G-24 provided the Vp/Vs background mudrock relation. Figure 3 demonstrates that the FRM of 18% Φ sand with in-situ (60%) gas saturation in M-41 plots in the same region as the known gas sand at the Annapolis G-24 discovery. This validates the FRM and porosity substitution as well as closing the AVO/LMR loop for flowable gas sand reservoir prediction.

Figure 4 shows the synthetic gathers generated from the FRM of 100% wet and 90% gas saturation for the in-situ 9% Φ case. The porosity was then increased to18% while maintaining the same sand thickness and fluid substitution was rerun for 100% wet and 60% gas saturation. The AVO response for the in-situ sand is a dim AVO class 1-2 with only a subtle change for increased 90% gas substitution. By contrast, the 10m, 18% Φ sand with in-situ 60% gas saturation produced a very bright class 3-4 (increasing/flat gradient) AVO response that was distinguishable from the class 5 (decreasing gradient) 18% Φ wet response.

A wedge model of AVO synthetic gathers was run to compare the 9% Φ and 18% Φ in-situ gas case, in 5m thickness increments, varying from zero to 50m (left to right panels in Figure 5). The results show that for the 9% Φ gas case, only negligible changes to the dim AVO response are seen even at fully-resolved thicknesses. The 18% Φ gas sand however, is quite bright at the 10m in-situ thickness and continues to brighten with increasing thickness. These encouraging

results from the modelling/fluid substitution feasibility work provided the impetus to proceed with the AVO/LMR inversion.

Flat-Spot AVO Classification, Modelling and LMR Attribute Analysis

Many claims have been made for post-stack interpretation of flat, cross-cutting events as fluid contacts. However, the AVO basis for these claims is either rarely investigated or the theoretical AVO type classifications for fluid-only contacts are flawed (Isaacson and Neff 1999). Figure 6 shows an Rp vs. Rs (P- and S-reflectivity) “circle” plot with the standard top reservoir AVO classes 1 to 5 and the new AVO fluid- only hydrocarbon/water contact (HWC) AVO class 6. The location and AVO gradient response of this HWC class 6 is established from the fact that a fluid change alone produces little or no change in shear impedance contrast, Rs. So the GWC in this DHI case is located only on the +ve Rp axis at near zero Rs. The resulting theoretical AVO gather response is a slight +ve R(zero°) with a slightly increasing gradient.

Angle stacks through the postulated DHI show significant brightening with offset for the trough-peak pair up-dip from the flat-spot (Figure 7). This AVO class 3-4 response matches the modelled response for an18% Φ gas-saturated sandstone (Figure 4). However the critical confirmation of the AVO class 3-4 gas sand response is provided by the correct AVO class 6 response for the flat spot at the down-dip GWC in the sand body (see figure 7, red box within top/base sand horizons). Based on this encouraging and exacting AVO class 6 requirement, it was decided to use this DHI as a fluid template for the $\lambda\mu\rho$-based analysis. It was found that the best ‘isolation’ of the DHI could be achieved by cross-plotting $\lambda\rho-\mu\rho$ difference versus P-impedance (Ip). Figure 8 shows this cross-plot for a line through the DHI flat-spot anomaly along with $\mu\rho$ sections. Selection of the black polygon on the periphery of the background shale perfectly isolates the DHI on the $\mu\rho$ section (Figure 8b). Note that the measured values for the 18% Φ gas sand in the G-24 well fall within this polygon. The application of the polygon mask to the data then isolates other LMR anomalies throughout a 2D grid of lines selected from the 3D.

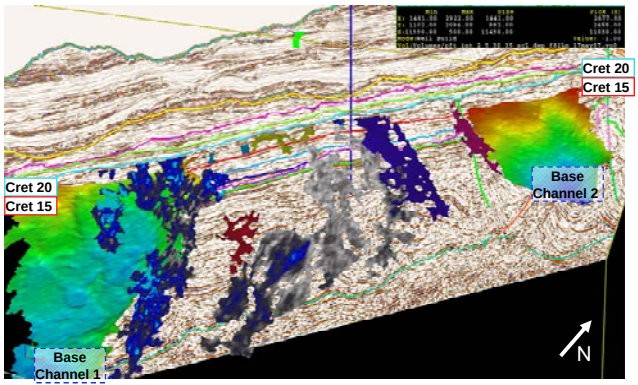

Figure 1: 3D Line:Cret.15-20 U.Missisauga channels/geobodies

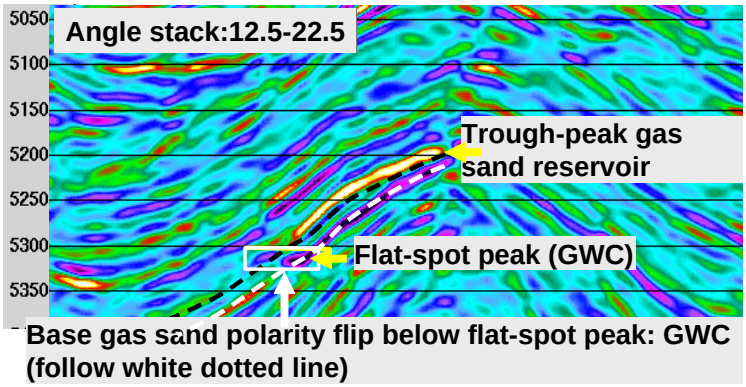

Figure 2: postulated DHI flat-spot mapped from 3D PSDM

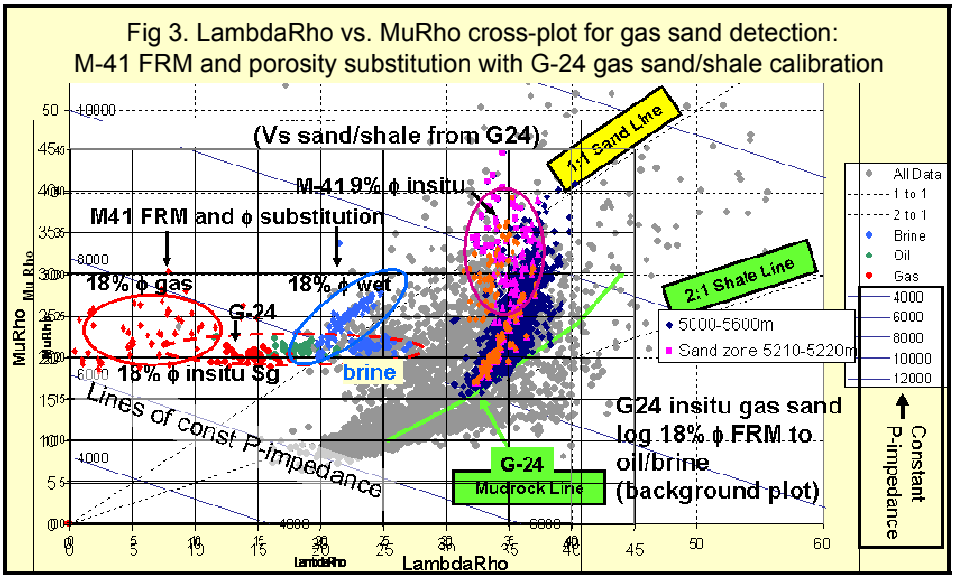

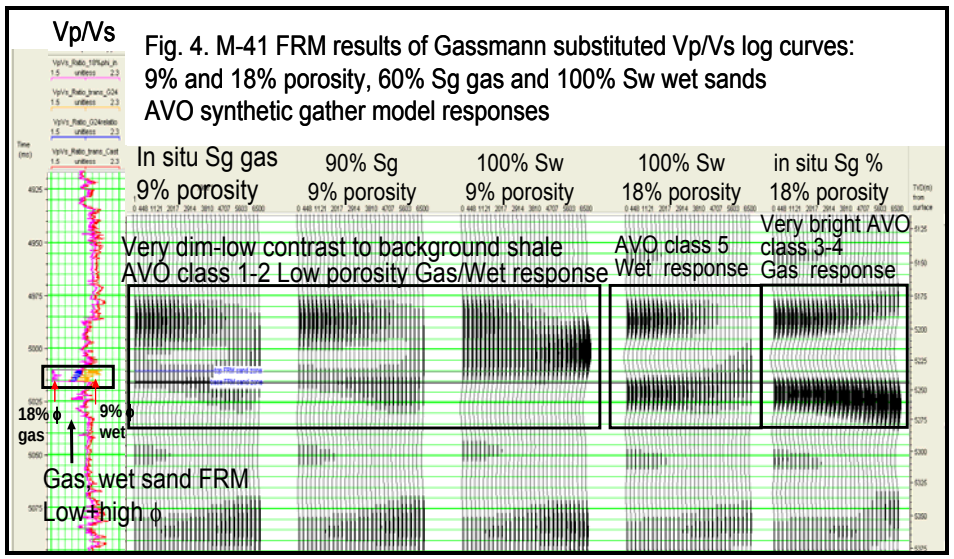

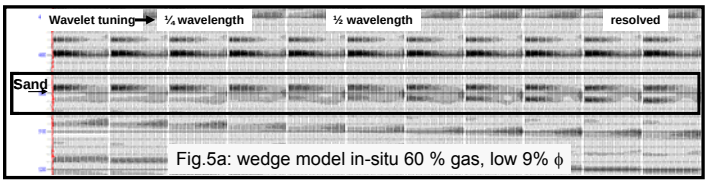

Fig.5a: wedge model in-situ 60 % gas, low 9% ϕ

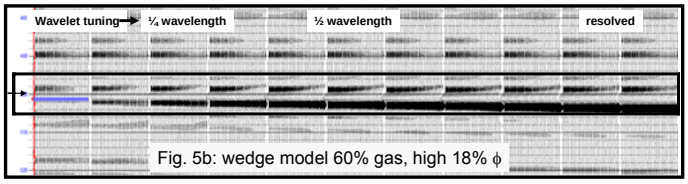

Fig. 5b: wedge model 60% gas, high 18% ϕ

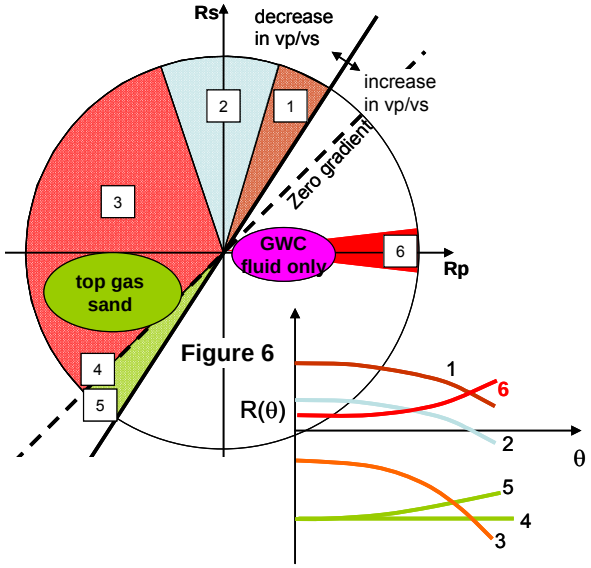

Figure 6: Rp vs Rs x-plot and AVO classes for gas sand and DHI GWC fluid response

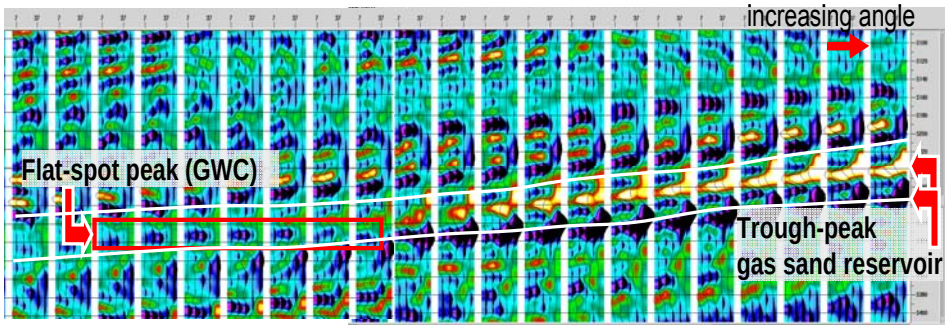

Figure 7: Strong AVO class 3 trough-peak gas sand up dip from weak flat-spot peak with slight increasing gradient i.e. correct AVO class 6 response

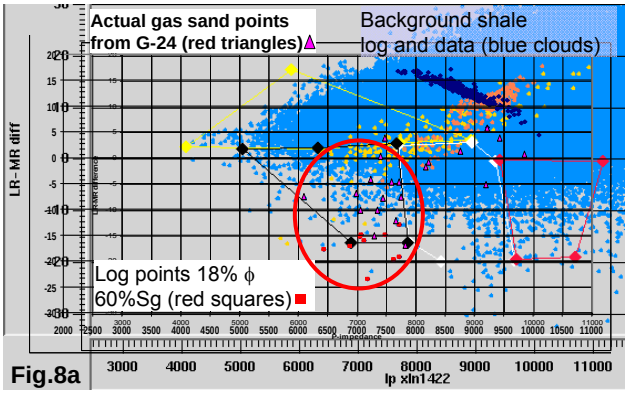

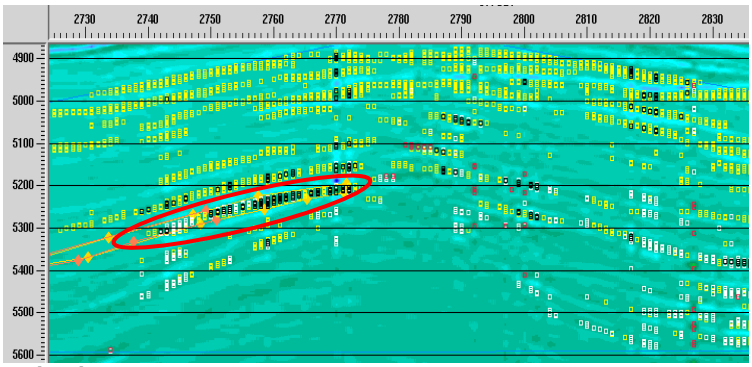

Figure 8a: Best DHI 'isolation' seen by cross-plotting log and seismic $\lambda\rho-\mu\rho$ difference vs P-impedance (Ip).

Figure 8b: 3D line result of clearly isolating the DHI+flat-spot anomaly using the black cross-plot polygon points from 8a.

Whilst successful, the Ip/LR-MR difference cross-plot analysis and volume mask was only available for a 2D grid of lines in time. Consequently, driven by the need to utilize the benefit of the full 3D volume in depth, it was decided to see if 3D, AVO intercept/gradient (IG) analysis and volume reconnaissance masking would produce satisfactory results. Again, the DHI flat-spot anomaly was used as a template test. A comparison of the mask results achieved by Ip vs. $\lambda\rho$-$\mu\rho$ difference and IG analysis on the flat-spot control, shows that the IG approach satisfactorily isolated the top and base of the gas sand DHI and also provided more discrete anomalies with less spurious attribute chatter. A 3D IG-based top/base reservoir sand mask depth volume was subsequently created and imported into GeoProbe for further analysis.

AVO geo-anomalies were then generated from this masked volume using an appropriate minimum of connected voxels. These were tracked as top and base pairs which corresponded to a trough over a peak, as per the modelled reflection response for a porous, gas-charged sand. As an additional check, gathers through these anomalies were analysed to confirm the 'correct' polarity. The geo-anomalies were re-exported to SeisWorks to infill the Ip vs. $\lambda\rho$- $\mu\rho$ difference 2D grid and provided a full 3D volume coverage. The final combined areas were used to help calculate volumetrics for the five target horizons. The reservoir risk element was modified by the assessed quality of the AVO anomalies at each horizon and resulted in a geological chance of success varying from 9% to 27% at the five levels. As a result of the work, the reservoir chance of success assigned to the primary objective interval was increased from 40% to 60%.

Conclusions

AVO and LMR analysis has been successful in mitigating reservoir risk at Stonehouse. FRM and porosity substitution work showed that the required high porosity gas sands would produce bright, class 3-4 AVO responses that would clearly distinguish them from the high porosity wet and low porosity wet or gas cases. A DHI with a new AVO type 6 fluid contact was defined and LR-MR vs. AI cross-plotting showed that it plotted within the same polygon as the measured 18% Φ gas sand in Annapolis G-24. The anomaly was also successfully isolated using 3D AVO, IG analysis and using this calibration, a top/base reservoir sand mask depth volume was created and imported to GeoProbe for analysis. A significant number of AVO geo-anomalies were generated at the objective horizons and used for volumetric and risking analysis. The positive AVO results for the principal Upper Missisauga interval resulted in a significant reduction in the reservoir risk.

Acknowledgements

The authors wish to thank EnCana management for allowing the presentation of this material.

References

Isaacson, E.S., and Neff, D.B., 1999. A B AVO cross plotting and its application in Greenland and the Barents Sea: Petroleum Geology of N.W. Europe: Proceedings of the 5th Conference: The Geological Society of London, **Vol 2**, 1289-1298.

Mojesky, T., Karagul, A., Goodway, W., Szelewski, C., and Dashwood, M., 2007. Reprocessing the E.Coast Canada Stonehouse Survey with 3D SRME and Hybrid Layer Tomography PreSDM: 2007 CSEG-CSPG Convention Abstracts.